JOURNAL OF THE ROYAL SOCIETY Interface

rsif.royalsocietypublishing.org

Research

Cite this article: Sareh S, Rossiter J, Conn A, Drescher K, Goldstein RE. 2013 Swimming like algae: biomimetic soft artificial cilia. J R Soc Interface 10: 20120666.
http://dx.doi.org/10.1098/rsif.2012.0666

Received: 17 August 2012
Accepted: 3 October 2012

Subject Areas:
biomimetics

Keywords:
biomimetics, artificial cilia, piecewise constant-curvature actuator

Author for correspondence:
Sina Sareh
e-mail: s.sareh@bris.ac.uk

Royal Society Publishing
Informing the science of the future

Swimming like algae: biomimetic soft artificial cilia

Sina Sareh[1], Jonathan Rossiter[1], Andrew Conn[2], Knut Drescher[3] and Raymond E. Goldstein[3]

[1]Department of Engineering Mathematics, and [2]Department of Mechanical Engineering, University of Bristol, Bristol BS8 1TR, UK
[3]Department of Applied Mathematics and Theoretical Physics, University of Cambridge, Cambridge CB3 0WA, UK

Cilia are used effectively in a wide variety of biological systems from fluid transport to thrust generation. Here, we present the design and implementation of artificial cilia, based on a biomimetic planar actuator using soft-smart materials. This actuator is modelled on the cilia movement of the alga *Volvox*, and represents the cilium as a piecewise constant-curvature robotic actuator that enables the subsequent direct translation of natural articulation into a multi-segment ionic polymer metal composite actuator. It is demonstrated how the combination of optimal segmentation pattern and biologically derived per-segment driving signals reproduce natural ciliary motion. The amenability of the artificial cilia to scaling is also demonstrated through the comparison of the Reynolds number achieved with that of natural cilia.

1. Introduction

Cilia are active organelles that are used by most eukaryotic organisms to move fluids. While micro-organisms use cilia to swim through fluids [1], higher organisms use cilia to control internal fluid motion, for example to transport mucus within the bronchial system [2]. Multicellular organisms often use many closely packed cilia that synchronize to collectively achieve a much-enhanced fluid motion [3], or to achieve organism-level coordination that is robust to the failure of individual cilia [4]. Cilia are usually between 1 and 20 μm long and move fluids by an asymmetric beating cycle that is efficient in very viscous environments. This ciliary movement is achieved by bending the whole filament, triggered by dynein molecular motors that slide the internal microtubules along each other. Remarkably, the cilia used by simple micro-organisms are structurally almost identical to those used by higher organisms, suggesting that millions of years of evolution have driven naturally occurring cilia to be the optimal elements for moving fluids at microscopic length scales. This has led to a number of efforts to replicate ciliary kinetics in micro-systems. These have predominantly focused on simple symmetric bending actuators driven by electrical [5,6] and magnetic [7,8] means. Unfortunately, these prior efforts have yielded little insight into the effectiveness of biomimetic artificial cilia that closely replicate the articulations of natural cilia. The ubiquity of biological cilia and wide variety of uses that Nature has found for them indicate that biomimetic artificial cilia would be extremely beneficial additions to the engineering and robotics domain. In the robotic community, the versatility of flexing actuators has long been studied, with particular focus on the generic class of hyper-redundant robot manipulators. The best examples of practical and biomimetic highly redundant (constrained hyper-redundant) manipulators are embodied by the work of Hirose, especially snake models, including ACM-R5 [9] and the SnakeBot [10]. Here, a large number of degrees of freedom (DOF), emerging from the serial connection of multiple rigid segments, are exploited to generate a range of snake-like ambulatory and manipulation motions. The contrast between these rigid-segment robots with the continuous flexible structures in nature has also led to the development of soft 'continuum'

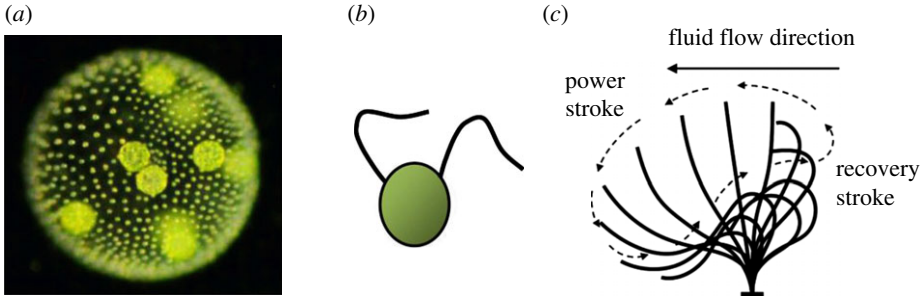

Figure 1. (*a*) *Volvox carteri* (reproduced with permission from Drescher *et al.* [4]), (*b*) the structure of a single biflagellate somatic cell within the *Volvox* colony, (*c*) schematic derived from the asymmetric flexural motion exhibited by a single *Volvox* cilium. (Online version in colour.)

robots. Soft continuum robotic manipulators are typically designed for manipulation in unstructured and cluttered workspaces [11,12]. Most of these manipulators are large industrial designs and are not amenable for adaptation into artificial cilia. By contrast, the relatively new field of electroactive polymers offers the potential to yield compliant actuators which can be fabricated at the meso- and micro-scales and which can readily exhibit the continuous flexion and asymmetric bending of natural cilia.

In this paper, we present the analysis, design and development of artificial cilia, using artificial muscles constructed from electroactive polymers. The motions of natural cilia are studied, and a kinematic model is developed that uses the practical restriction of constant curvature within a finite number of flexible segments. A voltage-based actuation scheme is developed which is then mapped to a multi-segment actuator made from ionic polymer metal composites (IPMCs). Finally, the actuation of the natural cilia, the multi-segment constant-curvature model and artificial IPMC cilia are compared.

1.1. Biological cilia

Nature has devised many different ways to generate and control fluid flow. At sub-millimetre scales, viscosity-dominated flow regimes necessitate the adoption of drag-based propulsion. Therefore, the fluid manipulation mechanisms used by cilia and flagella are of particular interest for micro-robotic applications, whether the flow is used for propulsion (e.g. swimming robots) or mass transfer (e.g. prosthetic trachea). Although cilia and flagella have the same physiological structure, the two terms have been used to differentiate the type of cell on which they appear. For example, in some cells, flagella are long and are present individually or in pairs (as in *Volvox*), whereas in other cells, cilia are short and are present in much larger numbers (as in the human respiratory tract). In this study, we use the terms interchangeably. Cilia range in size from less than 1 μm to 2 mm (although they are predominantly <20 μm) and typically beat at approximately 20–30 Hz [1]. They are highly effective at regulating fluid flows through confined geometries in biological vessels [13,14]. An individual cilium moves in an asymmetric manner so that a lateral unidirectional fluid flow is generated (figure 1*c*). The movement cycle of a cilium includes a large power stroke and a compressed recovery stroke. During the power stroke, the cilium is almost straight and its effect on the fluid is maximized, while during the recovery stroke the cilium flexes to minimize drag forces. In this study, we consider the colonial green alga *Volvox*, which consists of thousands of somatic cells embedded in the surface of an extracellular matrix, and a few germ cells inside the colony. The somatic cells on the *Volvox* surface are each endowed with two flagella that are oriented in the same direction (figure 1*b*), and beat with a characteristic cycle shown in figure 1*c*. The collective beating of the flagella on these somatic cells makes *Volvox* a highly motile organism, capable or navigating to nutrient and light sources in stagnant ponds and ditches. Directed motion of *Volvox* requires the coordination of the thousands of cells on the colony surface without a central nervous system, which is achieved by a modulation of the beating frequency in response to external stimuli [4,15].

1.2. Electroactive polymers for artificial cilia

Electroactive polymers are the set of relatively recent technologies within the general group of smart materials. Smart materials exhibit a measureable response to an orthogonal stimulus. In electroactive polymers, the stimulus is electricity and the response is some mechanical deformation, such as contraction or flexion. There are many electroactive polymers that may be adapted for fabrication into artificial cilia, including dielectric elastomers, conducting polymers and IPMCs [16]. Dielectric elastomers exhibit planar expansion and therefore fabrication into cilia would require complex multi-segment bimorph structures. Conducting polymers are more suitable for cilia structures but, again, a bimorph structure is required and the typical response of conducting polymers is slower than IPMCs. IPMCs, in contrast, are the most promising class of electro-active polymers for cilia structures. They are well suited to these low-force applications, can generate the required large bipolar displacements without the need for a bimorph structure, and can be readily segmented to enable complex actuated shapes. A variety of novel mechanisms and devices, including micro-pumps, fish and snake robots, dust wipers, active catheters and grippers have already been proposed based on IPMC actuators for industrial and biomedical applications [17].

When subjected to an external voltage stimulus, IPMCs undergo ion migration-induced swelling near the negative electrode and shrinkage near the positive electrode, resulting in bending of the actuator. IPMCs can also act as mechanical-to-electrical transducers where mechanical deformations induce internal ion migration and thereby generate a measureable current. Low driving voltages (<3 V), scalability, redundant DOF, chemical stability and silent operation are among the main motivations for using this promising class of actuators as an alternative propulsive system to conventional motors [17,18]. IPMCs typically work in liquid environments as the mobility of cations in the polymer network plays an essential role in their actuating and sensing

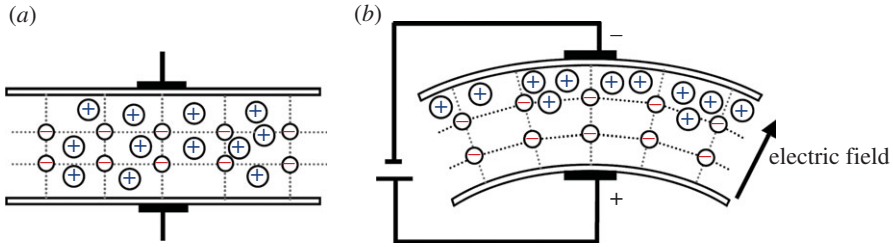

Figure 2. Principles of actuation in IPMC actuators (*a*) no input voltage and (*b*) voltage applied. (Online version in colour.)

principles. When an electric field is applied to the IPMC, unbound cations move in the direction of the electric field. This migration, and the associated parasitical water flux, generates a pressure imbalance across the material and a significant bending response [19] (figure 2*a*,*b*). Note that the bending of an ideal IPMC (where electrodes have zero resistance) is uniform along its length, resulting in an arc of constant curvature. Typically, IPMCs are composed of a thin (<0.5 mm) Nafion or Flemion membrane, with chemically deposited gold or platinum electrodes [20]. IPMCs can be fabricated at a nanometre scale and are still able to operate at a few microvolts [21]. Biocompatibility [22] and the considerable bending response in low-viscosity liquid environments make IPMCs suitable candidates for biorobotics applications. The similarity between natural cilia and IPMCs in terms of localized bending actuation, operation in water and wide scalability means that the IPMCs are excellent candidate materials upon which to base an artificial cilium. Hence, in the remainder of this paper, we will use only IPMC electroactive polymers in the design, fabrication and evaluation process.

Segmentation of the surface electrodes enables actuation of an IPMC into more complex shapes through the separate control of each segment. The segmentation approach has been used effectively to create a snake-like swimming robot [23], complex motion patterns, i.e. S-shaped actuation [24] and a soft three-link manipulator with visual feedback [25]. In this paper, we take advantage of the segmentation approach to design a ciliary actuator with piecewise constant curvature.

2. Identification of the complex motion of natural cilia

In order to generate a biologically realistic model of the motions of natural cilia, we focus on the kinematics of a single cilium on the surface of *Volvox carteri* f. *nagariensis* EVE [4]. A movie was taken of a single *Volvox* colony in the second half of its 48 h life cycle. A schematic of this life cycle is shown in Solari *et al*. [26]. The cilium studied in this paper was close to the anterior pole of the *Volvox* colony.

Twenty-four equally spaced frames from the movie showing the typical ciliary motion during one complete cycle at 25 Hz are shown in figure 3. It is clear that the *Volvox* cilium is approximately straight over the power stroke ($t_1 - t_{12}$) and curled during the recovery stroke ($t_{13} - t_{24}$) to minimize the drag force [27]. While the cilia motion in *Volvox* is not absolutely planar and has a small out-of-plane component [28], in this paper, we seek to replicate only the planar motion of cilia.

Kinematic data were extracted, using a custom application in Matlab, and the resulting 24 curves are shown in figure 4*a*, where the cilium is shown in horizontal orientation and is fixed at point (0,0). The curves are numbered to match the frames in figure 3, and the endpoints are clearly marked. The closed path encompassed by the 24 endpoints also shows the asymmetric beating of the *Volvox* cilia with power stroke (points 1–12) and recovery stroke (points 13–24) clearly visible.

To generate a kinematic model of the cilium which can be readily mapped to a soft robotic actuator, such as an IPMC, we need to consider the complexity of cilia beating in relation to the physical implementation constraints. These include a fixed number of segments and the constant curvature bending within each segment of the actuator. To this end, it is desirable to determine along the natural cilium the segments of curvature that have the same polarity of curvature, i.e. we wish to determine curvature inflection points. In this way, we may make an initial estimate of how many segments will be required in the artificial cilium. Subsequently, we consider flexion in the natural cilium where relatively distinct segments have differing curvatures, but which have the same bending polarity.

Analysis of the kinematics in figure 4*a* reveals that the natural cilium has a maximum of two distinct inflection points. This is shown clearly in figure 4*b* where the 24 frames are displayed horizontally, the normalized position along the length of the cilium is shown vertically and the inflection points are shown mapped onto the length. For example, in frame 1, the cilium has a single inflection point approximately in the middle of its length, whereas in frame 17, there are two inflection points at approximately 0.25 and 0.8, respectively. The most important observation from figure 4*b* is that the points of inflection are extremely mobile. Through the complete cycle, both inflection points travel from base towards the tip, with the second inflection point emerging only during the recovery stroke. This movement is illustrated in figure 4*b* by the arrows. Crucially, the dynamic segmentation in the natural actuator shown in figure 4*b* is not implementable in multi-link soft manipulators because segmentation points (and hence inflection points) are fixed at manufacture. In the following, we explain the principles of the soft multi-link manipulation architecture and show how we tackle the design problem of replicating natural cilia motion by making appropriate estimations based on the constraint of a fixed segmentation pattern.

3. Generalized multi-link soft manipulation model

We now present the framework for cilia representation under the restrictions of a fixed number of segments and where each segment exhibits a constant curvature along its length.

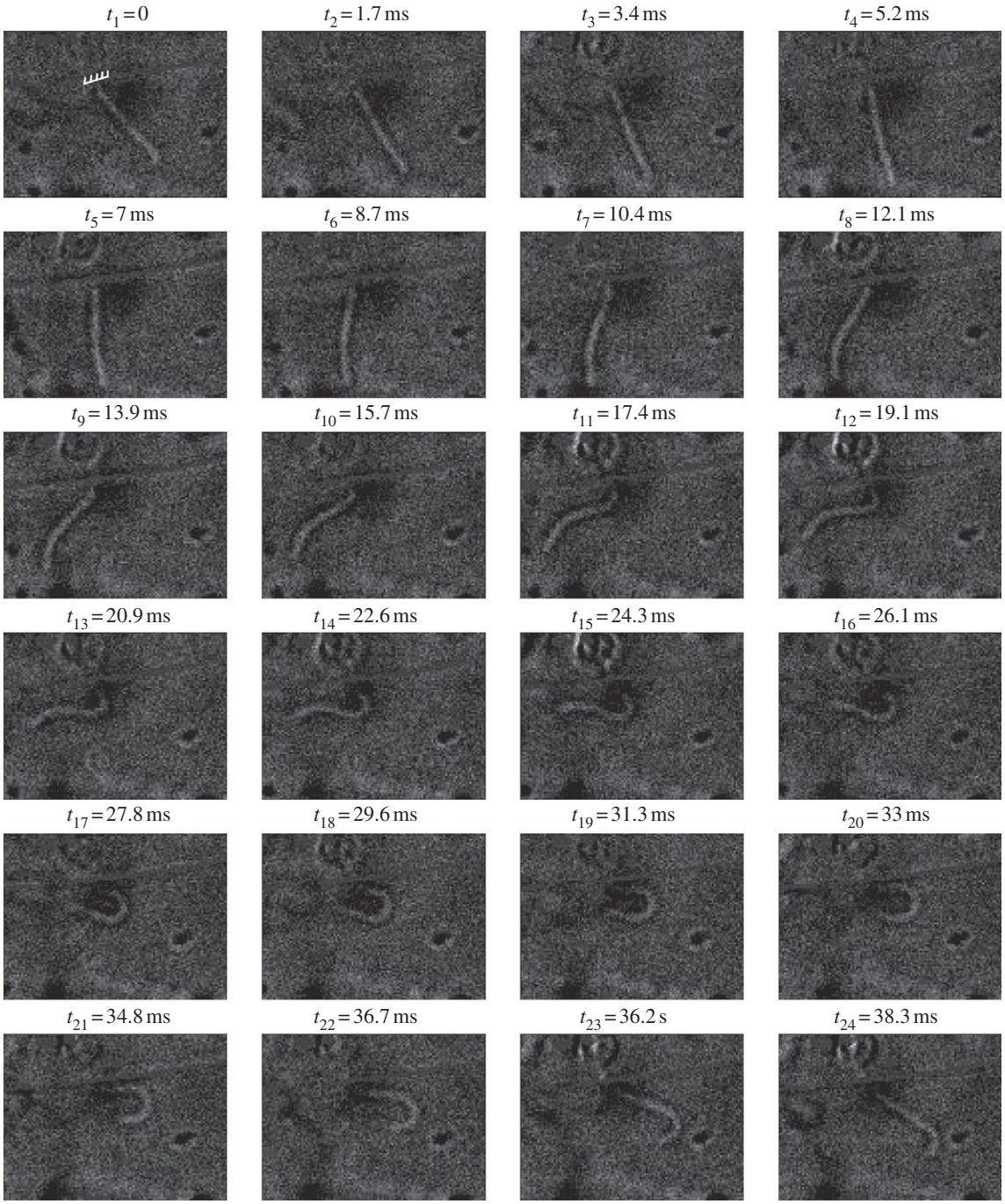

Figure 3. The natural beating pattern of a *Volvox* cilium at 25 Hz, fixed base of the cilium is shown in frame t_1.

Figure 5*b* illustrates an active soft structure as a series of bipolar constant-curvature segments (figure 5*a*). This is shown clearly, for example, where angle β_1 describes the endpoint deviation of segment l_1 with reference to its start point direction and φ_1 is the bending of the joint between segment l_1 and l_2. The piecewise constant-curvature architecture enables the whole cilium to be controlled through the application of a small number of independent signals [29].

Consider an ideal bipolar constant-curvature actuator as a perfectly circular curve of length l, tangent to the x-axis at its base. A positive input signal bends the actuator upwards so that its tip lies at the point P and its curvature fits on a circle of radius r with centre C (figure 5*a*). A negative input likewise bends the actuator downwards. Given sufficient input the actuator can bend into a perfect semicircle with radius l/π or even a perfect circle with radius $l/2\pi$. Referring to figure 5*a*, the actuator's tip position can be expressed as $P = (X_{\mathrm{p}}, Y_{\mathrm{p}})$ where,

$$X_{\mathrm{p}} = r\sin(\alpha), \qquad Y_{\mathrm{p}} = r(1-\cos(\alpha)). \tag{3.1}$$

The chord angle of the actuator, γ can be described as

$$\gamma = \tan^{-1}\left(\frac{Y_{\mathrm{p}}}{X_{\mathrm{p}}}\right). \tag{3.2}$$

Substituting X_{p} and Y_{p} from equation (3.1),

$$\gamma = \frac{\alpha}{2}, \tag{3.3}$$

and basic rules of geometry yield $\alpha = \beta$ and $\beta = 2\gamma$.

The unconventional joints-free structure of the proposed electroactive polymer soft actuators makes them

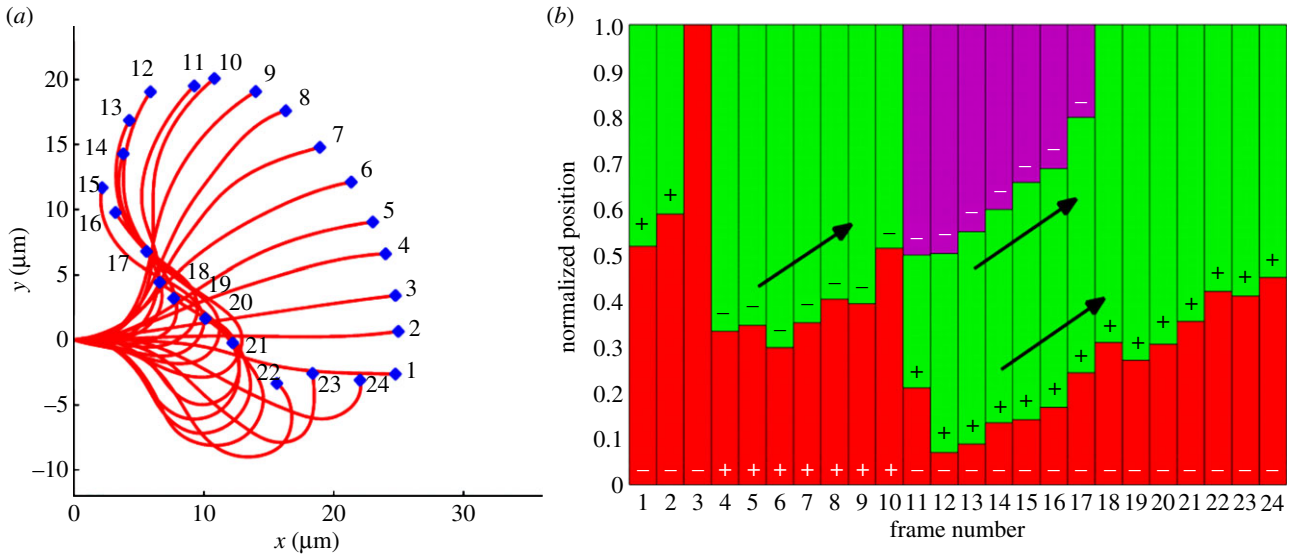

Figure 4. (*a*) The overlaid motion pattern extracted from a single *Volvox* cilium; (*b*) illustration of the dynamic segmentation pattern during the 24-frame sequence of cilia movement cycle. Arrows indicate the direction of displacement of the inflection points. (Online version in colour.)

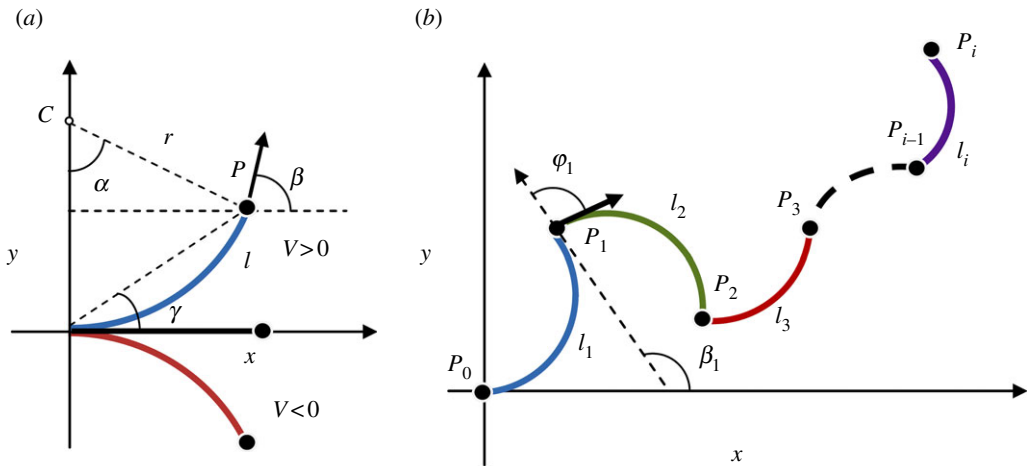

Figure 5. (*a*) Positive and negative bending of a single bipolar constant-curvature actuator of length *l* in response to voltage *V*; (*b*) schematic of the generalized soft multi-link manipulation with *i* segments [25]. (Online version in colour.)

fundamentally different from rigid link approximations and fully hyper-redundant robots. Hence, standard techniques for selecting frames of reference such as the Denavit–Hartenberg algorithm are not directly applicable for the kinematic analysis of soft robots [30]. In the following, we discuss a simple approach based on the earlier-mentioned arc geometry to compute kinematics of soft multi-link actuators.

Now consider a series of linked constant-curvature segments, as shown in figure 5*b*. Simple rotations and translations are sufficient to build up a full multi-segment structure. The tip positions of each segment, as defined by the points $P_0, P_1, P_2, \ldots, P_i$, are calculated from the previous segment as given in (3.4) where T_i is the transformation matrix to be applied to the endpoint P_i of segment i.

$$P_{i+1} = T_i P_i = \begin{bmatrix} \cos(\alpha_i + \varphi_i) & -\sin(\alpha_i + \varphi_i) & Xp_i \\ \sin(\alpha_i + \varphi_i) & \cos(\alpha_i + \varphi_i) & Yp_i \\ 0 & 0 & 1 \end{bmatrix} P_i. \quad (3.4)$$

Note that the curvature of any arbitrary segment bent with a radius of r_i can be calculated through $\alpha_i = l_i/r_i$, where l_i represents the length of that segment. Given all φi, the coordinates of any point along the actuator can be calculated using (3.4) and this relationship.

The transformation matrix T for the final endpoint of the manipulator can be computed by multiplying all transfer matrices from the base to the tip of the actuator [31]. For a three-segment actuator, the net transformation matrix can be expressed as $T = T_1\ T_2\ T_3$.

4. Optimization of actuator segmentation pattern

A cilium is capable of generating continuous complex deformation along its body. Mimicking this exact deformation in a multi-link soft actuator would require an extremely large number of very small segments. This is impractical from a number of points of view; the control system would be extremely complex and, given a finite gap between segments of the soft material (to ensure electrical separation), the proportion of the actuator that can actually move would diminish. As a compromise between the technological limitations and the biological inspiration, in this study we focus

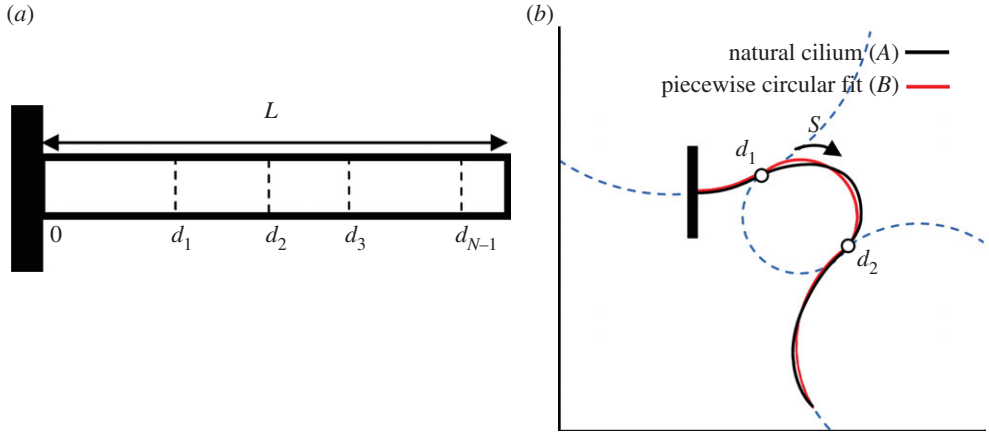

Figure 6. (*a*) Illustration of the segmentation pattern for an *N* segment actuator and (*b*) illustration of error used to form the cost function of the system for a three-segment actuator. The dashed circles illustrate the relative curvatures of the three circles that have been fit to the three segments. (Online version in colour.)

Table 1. The optimal segmentation parameters for multi-segment actuators ($L = 1$).

	optimal segmentation pattern					
number of segments	d_1	d_2	d_3	d_4	d_5	d_6
2	0.48					
3	0.30	0.61				
4	0.29	0.54	0.76			
5	0.18	0.35	0.56	0.77		
6	0.16	0.31	0.45	0.59	0.79	
7	0.17	0.31	0.45	0.58	0.75	0.90

on the implementation of an artificial cilium with limited number of segments, where the segmentation pattern is optimized to produce the most natural motion.

To enable this optimization, we define a cost function based on the accumulative error between the independent segments of natural cilia and the per-segment circular fit. This cost function is then minimized by applying a genetic algorithm optimization process in Matlab [32]. To form the cost function, the whole length of an IPMC actuator (L) is assumed to be divided into N segments conditioned as $d_1 < d_2 < d_3 ... < d_{N-1} < L$, where d_i marks the position of the segmentation boundary between segment i and segment $i + 1$, as illustrated in figure 6*a*. The set of parameters $\{d_1, \ldots, d_{N-1}\}$ is optimized by the genetic algorithm.

For a three-segment actuator, the argument that defines the segmentation pattern along the length of the actuator can be expressed as

$$d = \{d_1, d_2\}, \text{ where } 0 < d_1 < d_2 < L. \tag{4.1}$$

Referring to figure 6*b*, the error between the natural cilia segments and their idealized constant-curvature fit for a particular motion state and for a specific segmentation pattern $d = \{d_1, d_2\}$ can be simply considered as the summation of accumulated errors in three segments

$$\mathrm{e} = \sum_{s=0}^{l} \sqrt{(x_A(s) - x_B(s))^2 + (y_A(s) - y_B(s))^2}, \tag{4.2}$$

where $(x_A(s), y_A(s))$ and $(x_B(s), y_B(s))$ are the coordinates along the natural cilium and the piecewise constant-curvature fit, respectively, at position $0 \le s \le L$ along their lengths. Now we calculate the total error as the sum of error over all frames

$$E = \sum_{i=1}^{m} \mathrm{e}_i, \tag{4.3}$$

where m is the number of frames in the beating cycle (here $m = 24$).

Using the error function E in (4.3) as the genetic algorithm fitness function, the optimizer was run on six key states of the movement of cilia (every fourth frame in figure 4). The resulting optimal segmentation boundaries are shown in table 1 for ideal cilia actuators of length $L = 1$, ranging from 2 to 7 segments. For example, the first row shows that the optimal segmentation of a two-segment artificial cilium is a segmentation boundary at position 0.48, approximately halfway along the length.

An increase in the number of segments is expected to reduce overall error, because the artificial cilium will be more able to deform into the complex shape of the natural cilium. This is confirmed in figure 7*a*, which shows the total error for the segmentation schema in table 1. Here, the error is normalized with respect to the calculated absolute error for a single-segment actuator. There is a clear elbow in this graph where the number of segments is 3. After this point, the rate of reduction in error is very small. We therefore focus our work on the design and implementation of an artificial cilium with three separately controlled segments, as shown in figure 7*b*.

The simulation results in table 1 and figure 7*a* show that an ideal soft actuator, segmented into three independently

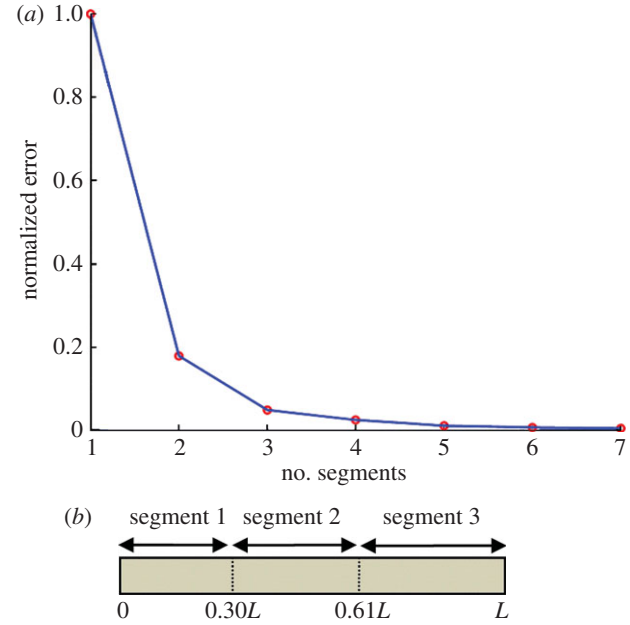

Figure 7. (*a*) The trend of error reduction as the number of segment is increased, and (*b*) the optimal segmentation pattern for a three-segment actuator. (Online version in colour.)

controlled segments at position $d_1/L = 0.3$ and $d_2/L = 0.61$, will have a normalized error of approximately 4.7 per cent. We can now apply this segmentation scheme to our constant-curvature soft actuation model to show how an artificial cilium can articulate in a manner very similar to the natural cilium. Figure 8 shows the three-segment soft manipulation model articulating into the six predominant states from figure 4 (i.e. every fourth frame). The dashed circles are shown to illustrate the three constant-curvature segments of the actuator. It is clear from figure 8 that a three-segment idealized artificial cilium can articulate closely into the shape of a natural cilium. Note that all segments are connected smoothly at the optimum segmentation points. This is consistent with the inter-segment mechanical constraints imposed by IPMC actuators and indicates that IPMCs are ideal candidates for the realization of artificial cilia.

5. Implementation of ionic polymer metal composite artificial cilia

Not only do the smooth connections between segments of the optimized soft manipulation model match those of the IPMCs (as outlined earlier) but they are also attractive from an analytical and control point of view. Considering $\varphi_i = 0$ for IPMC actuators, the configuration of the multi-link soft actuation is simplified as illustrated in figure 9. Each link represents an electrically isolated segment of the actuator while sharing a contiguous ion-exchange membrane with all other segments. In the remainder of the paper, we address the challenges regarding design adaptation and fabrication of the IPMC artificial cilium.

5.1. Characterization of bending in ionic polymer metal composites

An idealized IPMC has zero resistance across its surface electrodes and will bend with a constant curvature. Unfortunately, any real IPMC will have a non-zero electrode resistivity. For example, gold-plated IPMCs fabricated using the Oguro–Asaka method of electro-less chemical plating will typically have resistance less than 0.5 $\Omega\,\mathrm{cm}^{-1}$ [19]. This resistance results in a slight reduction in curvature along the length of the actuator. For simplicity, we assume the reduction in curvature is minimal and henceforth we model the IPMC as a constant-curvature actuator. In order to implement the multi-segment model above in a real IPMC, we initially characterize the voltage–curvature relationship for the fabricated Nafion 115 IPMCs. For this purpose, an IPMC strip of 50 × 4 mm, gold-plated Nafion 115 was fabricated with a total thickness of approximately 130 μm. The IPMC was fixed at one end and operated in water with a slow ramp-up and ramp-down voltage signal, with maximum voltage of 3.5 V. The IPMC actuation was captured with a high-resolution video camera, and a constant-curvature arc was fitted to the actuator profile. Figure 10 shows the relationship between curvature of bending and the excitation voltage for the IPMC.

A first-order exponential function was fit to the experimental data, using the nonlinear least-squares method and is shown in figure 10. Equation (5.1) defines the necessary relationship between curvature and voltage needed to implement multi-segment cilia-like structures in gold-plated Nafion 115 IPMCs.

$$r = 94.09\mathrm{e}^{-1.30V}. \tag{5.1}$$

5.2. Estimation of total actuator length

In order to fabricate an effective multi-segment IPMC artificial cilium that has the same shape as the natural cilium, we must first determine the minimum IPMC length needed to achieve the necessary total bending. The minimum length is clearly limited by the relationship in figure 10, which itself is determined by the IPMC ion-exchange membrane thickness, and also by the maximum permissible voltage that can be applied to the IPMC. We assume that a soft bending actuator driven by maximum voltage $V_{\max}$ bends with minimum radius of curvature $R_{\min}$. Therefore, for an n-segment actuator,

$$L_{\min} = R_{\min} \times \sum_{i=1}^{n} \alpha_i, \tag{5.2}$$

where $L_{\min}$ is the minimum length for the actuator, and α is segment angulation as shown in figure 5. Referring to figure 4, the maximum sum of absolute bending angle is approximately 270°. To achieve this total bending angle in a Nafion 115 IPMC, we refer to figure 10 and observe that the corresponding radius of 1.15 cm is possible at a maximum voltage of 3.4 V. Voltages above this value are likely to damage the IPMC or cause excessive electrolysis which can disrupt IPMC actuation. Substituting into (5.2), we estimate the minimum length of the Nafion 115 IPMC actuator needed to replicate the full range of natural cilia motions to be $L_{\min} \approx 6.4$ cm.

5.3. Electrode patterning for multi-link manipulation

To create sophisticated IPMC actuators capable of performing complex manipulation, we must segment the surface electrodes. This segmentation is achieved by cutting or otherwise partitioning the electrodes such that the polymer membrane

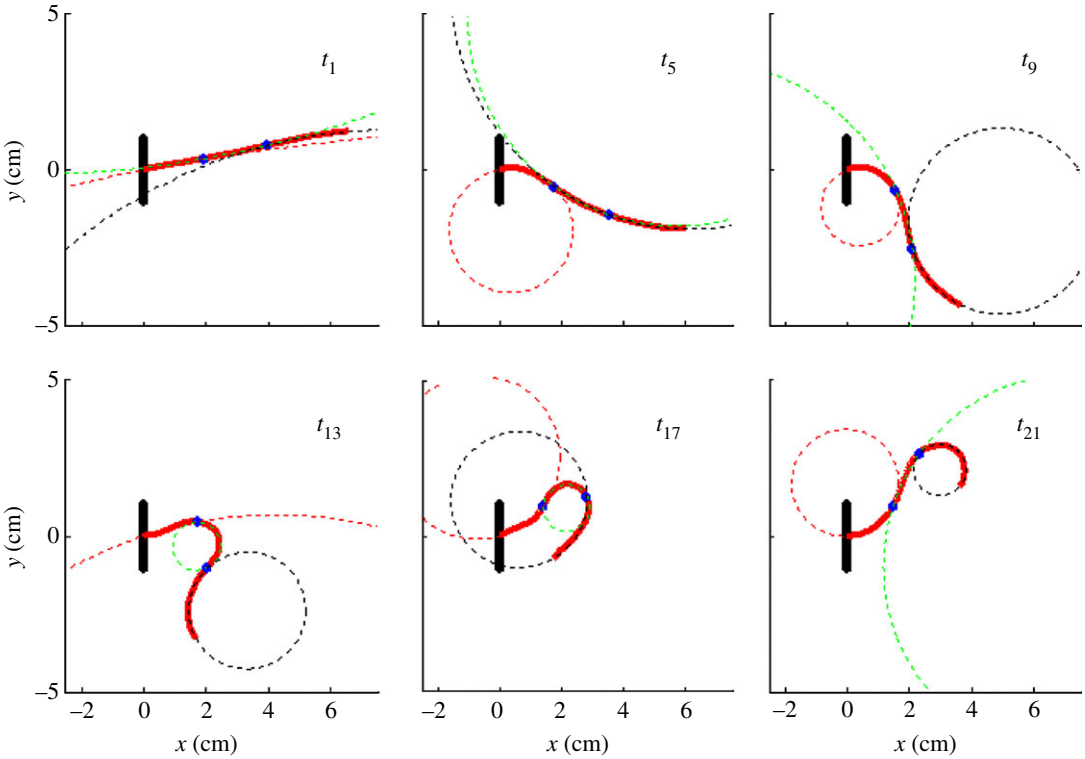

Figure 8. Piecewise constant-curvature estimation when the actuator is optimally segmented into three segments. Six prominent states of cilia movements are shown. Here $L = 6.4$ cm as discussed in §5.2. (Online version in colour.)

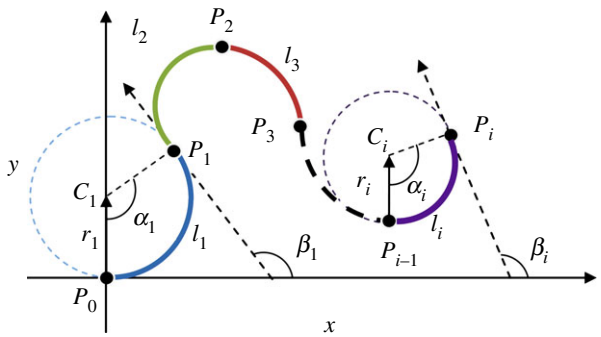

Figure 9. The multi-link soft manipulation model for IPMC actuators. (Online version in colour.)

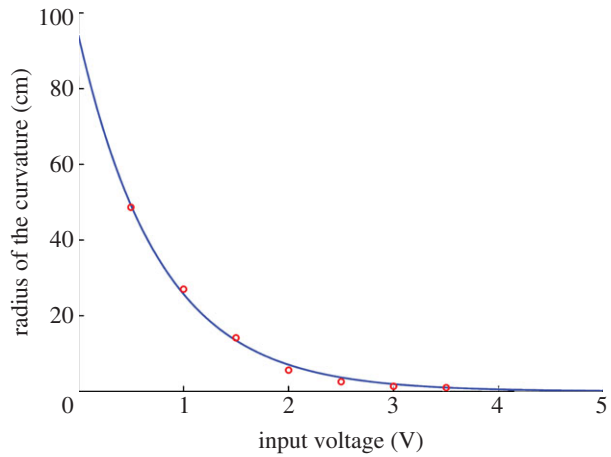

Figure 10. Change in radius of the curvature against input voltage for a Nafion IPMC and the exponential fit. Solid line, exponential fit; circles, experimental data. (Online version in colour.)

remains unaffected. To realize this segmentation, we use electro-discharge machining (EDM) to pattern the cilium actuator. EDM is a simple segmentation technique, which involves selective removal of surface electrode material through a sequence of very small spark discharge events. EDM is naturally self-limiting in terms of the applied mechanical pressure and consistency of the patterning speed [33]. The simulation results presented earlier suggest partitioning an IPMC strip with active length of $L = 6.4$ cm into three serially connected segments of 1.92, 1.98 and 2.50 cm from the base to tip of the actuator (i.e. $d_1/L = 0.3$ and $d_2/L = 0.61$).

Although the earlier-mentioned simulations suggest a segmentation pattern that is asymmetric along the length of the actuation, a symmetric actuator has a number of advantages. Because the symmetric actuator can be mounted in reverse, its lifetime may be extended by simply swapping ends. Additionally, a symmetric pattern also simplifies the experimental set-up when dealing with a large number of actuators, e.g. actuating a bundle of cilia in a coordinated fashion. We therefore modify the optimal design given above by adding an extra 2 mm to the shortest segment, to allow for the base mounting clip, and slightly shifting the central segment. The resulting pattern has three segments of length 2.3, 2 and 2.3 cm, respectively. The actuation error between the natural and the idealized IPMC model for our revised symmetric segmentation pattern is 5.2 per cent (an increase of <0.5%). This minimal increase in error was deemed a small penalty for the added flexibility of a symmetric actuator.

5.4. Bio-reconstruction of the excitation signals

Along with the optimized segmentation pattern obtained earlier, a set of appropriate excitation signals are needed to

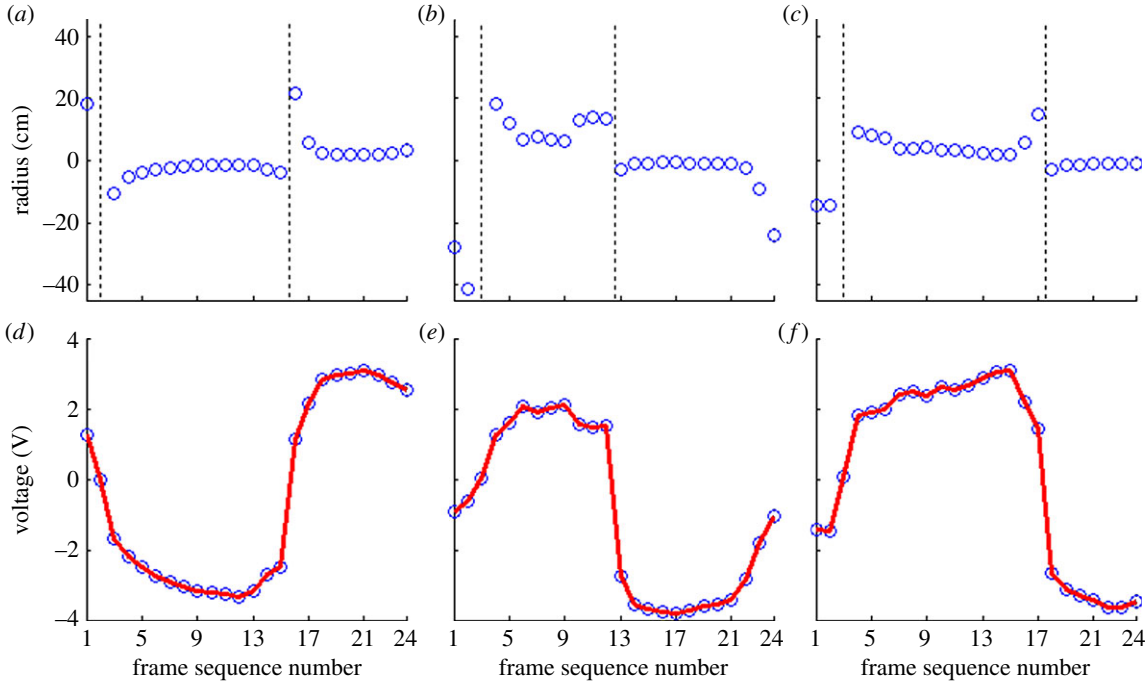

Figure 11. Sequential presentation of the change in the radius of each segment of the three-segment IPMC model over one cycle of movement, (*a*) base segment, (*b*) middle segment, (*c*) tip segment, and corresponding excitation signals (*d*) base segment, (*e*) middle segment, (*f*) tip segment. (Online version in colour.)

achieve the desired cilia-like motion. To calculate these signals, we examine the curvature of each segment in the IPMC model above as fitted to the natural cilium. The stimulation voltage required to achieve these curvatures was back calculated from the exponential radius–voltage relationship in (5.1).

The radii of curvature (top) and correlated excitation signals (bottom) for the full 24 frames of the IPMC cilia model are shown in figure 11. Note that the dotted lines in the radius profile plots are asymptotes of the radius, each representing a polarity change in both curvature and the input signal.

5.5. Simulation and actuation of the three-segment artificial cilium

Having prepared an optimally segmented IPMC actuator together with the corresponding reconstructed input signals, we now undertake a comparative study of the motion of the natural, simulated and experimental artificial cilia.

Reconstructed driving signals, as derived earlier, of frequencies {0.1, 0.2, 0.3, 0.4, 0.5} Hz were generated in Matlab and output through a National Instruments NI-PCI 6704 analogue output card. These low-power analogue signals were amplified using LM2726 power operational amplifiers (STMicroelectronics) with unity gain. The actuator was placed in the middle of a $50 \times 50 \times 20\ \text{cm}^3$ tank filled with deionized water. Each of the amplified control signals were delivered directly to the middle of each segment through lightweight copper wires and small spring clips. Figure 13*b* shows the IPMC in experimental configuration within the water tank. The profile of the actuator was recorded at each frequency and then analysed.

Applying the 0.1 Hz driving signals derived above to the idealized three-segment IPMC model results in the ciliate motion shown in figure 12*a*. Applying the same 0.1 Hz driving signals to the actual three-segment IPMC actuator results in the motion shown in figure 12*b*. Although there is a clear difference between the idealized (figure 12*a*) and actual (figure 12*b*) IPMC, these results show that the physical IPMC actuator generates a significant actuation cycle with a clear power and recovery stroke. The large area swept by the physical IPMC, and the large area encompassed by the path of the tip shown in figure 12*b* also indicate a significant directional fluidic interaction, confirming the effectiveness of our biomimetic approach.

Now let us consider the trajectory of the tip of the cilium in the three cases of (i) natural cilium; (ii) simulated IPMC cilium model; and (iii) physical artificial IPMC cilium. Figure 13*a* shows the tip trajectory of these three cases at the same 0.1 Hz and where the same driving signals are used for both the constant-curvature model and the artificial IPMC cilium. Note that the IPMC and natural cilia dimensions are normalized to the cilia length. To evaluate the difference between two trajectories, the swept-area error function (SE) is defined as the percentage of swept area encompassed by the tip trajectories that falls outside their intersection. The calculated swept-area error (SE) between the three cases of natural, simulated and artificial cilia is calculated as: $\text{SE}_{\text{natural,simulated}} = 19.9$ per cent, $\text{SE}_{\text{simulated,artificial}} = 28.3$ per cent and $\text{SE}_{\text{natural,artificial}} = 35.6$ per cent.

Khaderi *et al.* [7] have shown that the enclosed area that is swept by a cilium during one cycle of motion is linearly correlated to the volume of resulting displaced fluid. Osterman & Vilfan [34] also formulated this relationship for the single particle model of cilium. Similarly, Golestanian & Ajdari [35] have shown that the average velocity of a three-link sphere swimmer is proportional to the swept area. This correlation can be used as a measure of the effectiveness of cilia-like actuation for our artificial cilium. We extracted end tip trajectories for the artificial IPMC cilium at different actuation frequencies between 0.5 and 0.1 Hz. The areas encompassed by the trajectory of the tip of the artificial cilium for these frequencies are shown in figure 14*a*. Figure 14*b* shows the swept area per cycle as a function of frequency. This illustrates that decreasing the actuation

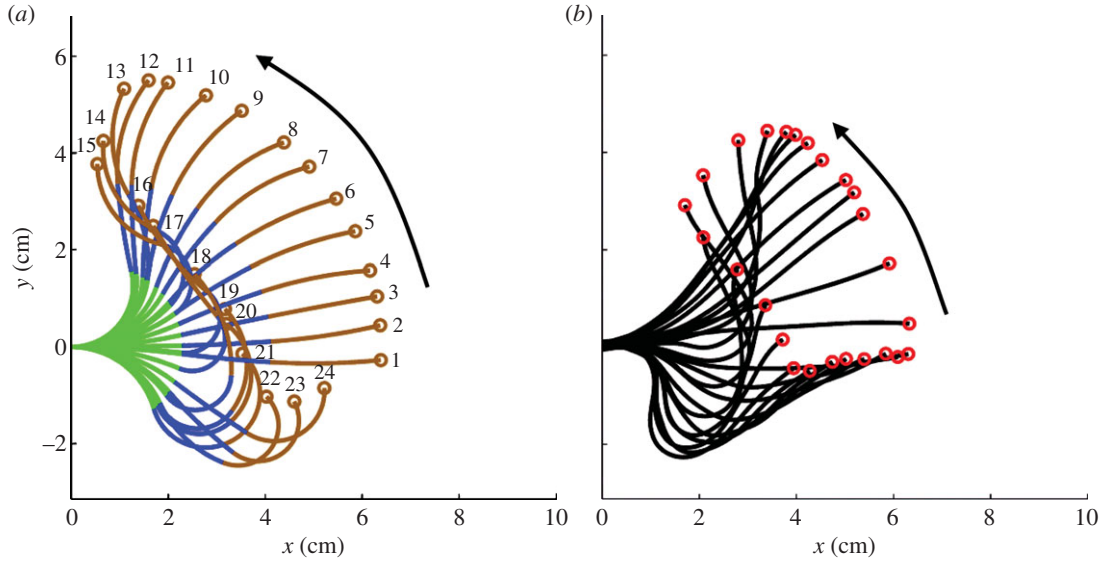

Figure 12. (*a*) The simulated motion pattern for a three-segment cilia actuator with symmetric segmentation pattern, (*b*) the experimental motion pattern extracted from the three-segment physical IPMC cilium at 0.1 Hz. (Online version in colour.)

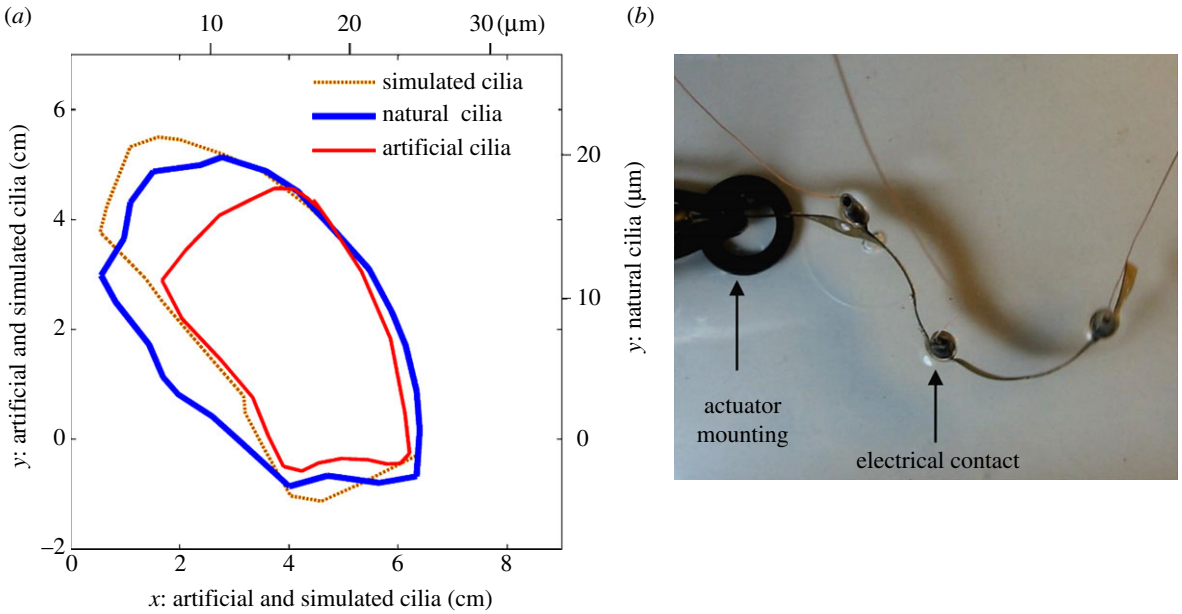

Figure 13. (*a*) Tip position trajectories obtained for natural, simulated and artificial cilia, (*b*) the IPMC artificial cilium actuator in experimental configuration. (Online version in colour.)

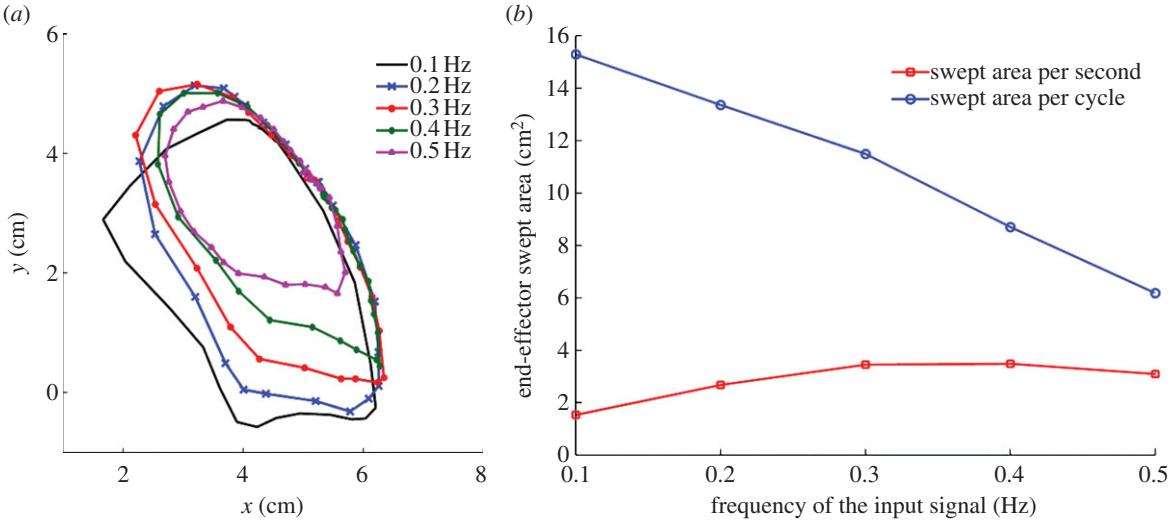

Figure 14. (*a*) Swept area of the tip of the artificial IPMC cilium driven at different frequencies, (*b*) The change in swept area with frequency. (Online version in colour.)

frequency increases the enclosed swept area with a near-linear relationship. Here, we have a clear trade-off between the size of any one actuation cycle and the frequency of operation. The total swept area over a 1 s period for the same frequencies is also illustrated in figure 14*b*. This shows clearly that although higher frequencies show reduced swept area per cycle the total swept area per second is highest for input frequencies around 0.3 Hz. This frequency can be interpreted as the resonance of the complete artificial cilia system, including electro-mechanical transduction of the IPMC and hydrodynamic interactions between the cilium and the water.

5.6. Dynamic similarity

To compare the hydrodynamic effects present in the small natural cilium and the larger artificial IPMC cilium, the Reynolds number for each was calculated. For flows caused by periodic motion such as the beating of cilia or pulsating blood flow, the Reynolds number is typically scaled in terms of the angular velocity

$$Re = \frac{\rho\omega\ell^2}{\eta}, \tag{5.3}$$

where ρ and η represent fluid density and dynamic viscosity and ω and ℓ are the angular velocity and length of the cilium, respectively [3,36,37]. The length of beating cilia in *Volvox* in this study is 25 μm (approx. 300 nm diameter) beating at 25 Hz. The length of our artificial cilium is 6.4 cm, actuating at 0.1 Hz, hence corresponding Reynolds numbers for motion in water are calculated as

$$Re_{\text{natural}} = 0.015, \tag{5.4}$$

and

$$Re_{\text{artificial}} = 409.6. \tag{5.5}$$

The higher Reynolds number in the artificial cilium implies the existence of a higher component of inertial force. In practical applications, we would ideally desire our artificial cilium to be of the same size and operate at the same frequency as the natural cilium. The fundamental scaling parameter of the IPMC in this study is the thickness of the Nafion 115 ion-exchange membrane, which effectively determines the voltage-induced curvature relationship in (5.1). It has been recently demonstrated by Lei *et al.* [38] that sub-millimetre IPMCs can be achieved by solvent casting Nafion in micro-fabricated silicon wafer moulds. Hence, ongoing work by the authors of this study is focusing on both this approach and other viable alternatives such as ultra short pulse laser cutting. Also, the inherent scalability of the EDM electrode segmentation technique can be exploited to ensure controllable segment lengths are maintained at smaller scales. On the other hand, larger cilia are useful for a wide variety of applications where dexterity and adaptability are required such as thrust generation in swimming robots, fluid control, object manipulation and active mixing.

6. Conclusion

We have presented a new soft robotic artificial cilium that replicates the motion of biological cilia. We have demonstrated how a biological cilium can be viewed as a piecewise constant-curvature manipulator and have introduced an analogous artificial muscle model to replicate the motion of natural *Volvox* cilia, using a finite number of constant-curvature segments. The analysis of the articulation of natural cilia suggests that although the most ideal actuator should have a reconfigurable segmentation pattern, a small number of fixed-length segments can capture the complex bending of the cilia to a relatively high degree. We fabricated an artificial three-segment IPMC cilium based on the fixed segmentation pattern obtained using global optimization. Biological data have also been used to derive suitable input signals to drive the three separately controlled segments. The artificial IPMC cilium has been evaluated at frequencies in the range of 0.1 to 0.5 Hz and shows a similar movement pattern to natural cilia.

The artificial cilia presented here can be used for a wide range of robotic applications, but is especially suited for controlling fluid flow and as a propulsive element for swimming robots. Future work will consider the fluid dynamics of the artificial cilia and the possibilities for miniaturization and metachronal wave formation through coordinated control of a bundle of cilia actuators.

The work was supported in part by the EPSRC and the ERC, through Advanced Investigator Grant 247333, and project grants EP/I032533/1 and EP/F022824/1.

References

1. Satir P. 1983 *Cilia and related organelles*, 3–9. Burlington, NC: Carolina Biological Supply Company.
2. Van der Schans CP. 2007 Bronchial muscus transport. *Respir. Care* **52**, 1150–1156.
3. Cartwright J, Piro O, Tuval I. 2004 Fluid-dynamical basis of the embryonic development of left–right asymmetry in vertebrates. *Proc. Natl Acad. Sci. USA* **101**, 7234–7239. (doi:10.1073/pnas.0402001101)
4. Drescher K, Goldstein R, Tuval I. 2010 Fidelity of adaptive phototaxis. *Proc. Natl Acad. Sci. USA* **107**, 11 171–11 176. (doi:10.1073/pnas.1000901107)
5. Nonaka S, Yoshiba S, Watanabe D, Ikeuchi S, Goto T, Marshall WF, Hamada H. 2005 *De novo* formation of left–right asymmetry by posterior tilt of nodal cilia. *PLoS Biol.* **3**, e268. (doi:10.1371/journal.pbio.0030268)
6. Oh K, Chung JH, Devasia S, Riley JJ. 2009 Biomimetic silicone cilia for microfluidic manipulation. *Lab. Chip* **9**, 1561–66. (doi:10.1039/b817409a)
7. Khaderi S, Baltusse M, Anderson P, Ioan D, Toonder J, Onck P. 2009 Nature-inspired microfluidic propulsion using magnetic actuation. *Phys. Rev. E.* **79**, 046304. (doi:10.1103/PhysRevE.79.046304)
8. Evans BA, Shields AR, Lloyd Carroll R, Falvo MR, Washburn S, Superfine R. 2007 Magnetically actuated nanorod arrays as biomimetic cilia. *Nano Lett.* **7**, 1428–1434. (doi:10.1021/nl070190c)
9. Yamada H, Chigisaki S, Mori M, Takita K, Ogami K, Hirose S. 2005 Development of amphibious snake-like robot ACM-R5. *Proc. 36th Int. Symp. Robotics* **36**, 133.
10. Lipkin K, Brown I, Peck A, Choset H, Rembisz J, Gianfortoni P, Naaktgeboren A. 2007 Differentiable and piecewise differentiable gaits for snake robots. In *Proc. IEEE Int. Conf. Intelligent Robots and Systems, 1864–1869. San Diego, CA, 29 October to 2 November 2007*. Piscataway, NJ: IEEE.
11. Cowan L, Walker I. 2008 Soft continuum robots: the interaction of continuous and discrete elements. In *Artificial life XI: Proc. 11th Int. Conf. Simulation and*

Synthesis of Living Systems (eds S Bullock, J Noble, R Watson, MA Bedau), pp. 126–133. Cambridge, MA: MIT Press.

12. Trivedi D, Rahn C, Kier W, Walker I. 2008 Soft robotics: biological inspiration, state of the art, and future research. *Appl. Bionics. Biomech.* **5**, 99–117. (doi:10.1080/11762320802557865)
13. Vogel S. 1994 *Life in moving fluids*. Princeton, NJ: Princeton University Press.
14. Alexeev A, Yeomans JM, Balazs AC. 2008 Designing synthetic, pumping cilia that switch the flow direction in microchannels. *Langmuir* **24**, 12 102–12 106. (doi:10.1021/la801907x)
15. Kirk D. 1998 *Volvox: a search for the molecular and genetic origins of multicellularity and cellular differentiation*. Cambridge, UK: Cambridge University Press.
16. Bar-Cohen Y, Kim KJ, Choi HR, Madden JDW. 2007 Electroactive polymer materials. *Smart Mater. Struct.* **16**, 2.
17. Shahinpoor M, Kim KJ. 2005 Ionic polymer-metal composites.: IV. Industrial and medical applications. *Smart Mater. Struct.* **14**, 197–214. (doi:10.1088/0964-1726/14/1/020)
18. Ko B, Kwon Hyok C, Lee S. 2008 A self-sensing method for IPMC actuator. *Adv. Sci. Technol.* **56**, 111–115. (doi:10.4028/www.scientific.net/AST.56.111)
19. Punning A, Kruusmaa M, Abaloo A. 2007 Surface resistance experiments with IPMC. *Sens. Actuators A* **133**, 200–209. (doi:10.1016/j.sna.2006.03.010)
20. Jung K, Nam J, Choi H. 2003 Investigations on actuation characteristics of IPMC artificial muscle actuator. *Sens. Actuators A* **107**, 183–192. (doi:10.1016/S0924-4247(03)00346-7)
21. Shahinpoor M. 2008 Ionic polymer conductor nanocomposites (IPCNCs) as distributed nanosensors and nanoactuators. *Adv. Sci. Technol.* **54**, 70–81. (doi:10.4028/www.scientific.net/AST.54.70)
22. Chen Z, Shen Y, Xi N, Tan X. 2007 Integrated sensing for ionic polymer-metal composite actuators using PVDF thin films. *Smart Mater. Struct.* **16**, S262–S271. (doi:10.1088/0964-1726/16/2/S10)
23. Rossiter J, Stoimenov B, Nakabo Y, Mukai T. 2006 Three-phase control for miniaturization of a snake-like swimming robot. In *Proc. 2006 IEEE Int. Conf. Robotics and Biomimetics*. *Kunming, China. 17–20 December 2006*. Piscataway, NJ: IEEE.
24. Stoimenov BL, Rossiter JM, Mukai T. 2007 Manufacturing of ionic polymer metal composites (IPMCs) that can actuate into complex curves. In *Proc. SPIE Electroactive Polymer Actuators and Devices* (*EAPAD*)**6524**, 65240T.
25. Nakabo Y, Mukai T, Asaka K. 2005 Kinematic modeling and visual sensing of multi-DOF robot manipulator with patterned artificial muscle. In *Proc. 2005 IEEE Int. Conf. Robotics Automation* (*ICRA2005*) 4326–4331. See http://ieeexplore.ieee.org/stamp/stamp.jsp?arnumber=01570784.
26. Solari CA, Drescher K, Ganguly S, Kessler JO, Michod RE, Goldstein RE. 2011 Flagellar phenotypic plasticity in volvocalean algae correlates with Péclet number. *J. R. Soc. Interface* **8**, 1409–1417. (doi:10.1098/rsif.2011.0023)
27. Gray J. 1928 *Ciliary movement*. Cambridge, UK: Cambridge University Press.
28. Hoops H. 1993 Flagellar, cellular and organismal polarity in *Volvox cateri*. *J. Cell Sci.* **104**, 105–117.
29. Webster III R, Jones B. 2010 Design and kinematic modeling of constant curvature continuum robots: a review. *Int. J. Robot. Res.* **29**, 1661–1683. (doi:10.1177/0278364910368147)
30. Giri N, Walker ID. 2011 Three module lumped element model of a continuum arm section. *Proc. IROS* **2011**, 4060–4065.
31. Kim K, Tadokoro S. 2007 *Electroactive polymers for robotic applications*, 1st edn. Springer.
32. Chipperfield A, Fleming P, Pohlheim H, Fonsec C. 1994 *Genetic algorithm toolbox for use with Matlab* (*v1.2*). Sheffield, UK: Department of Automatic Control and Systems Engineering, University of Sheffield.
33. Rossiter J, Mukai T. 2011 Electrostatic and thermal segmentation of multi-segment IPMC Actuators. *Proc. of SPIE* **7976**, 1–8. (doi:10.1117/12.880410).
34. Osterman N, Vilfan A. 2011 Finding the ciliary beating pattern with optimal efficiency. *Proc. Natl Acad. Sci. USA* **108**, 15 727–15 732. (doi:10.1073/pnas.1107889108)
35. Golestanian R, Ajdari A. 2008 Analytic results for the three-sphere swimmer at low Reynolds number. *Phys. Rev. E* **77**, 036308. (doi:10.1103/PhysRevE.77.036308)
36. Blake J. 1973 Flow in tubules due to ciliary activity. *Bull. Math. Biol.* **35**.
37. Niklas K. 1994 *Plant allometry: the scaling of form and process*. Chicago, IL: The University of Chicago Press.
38. Lei H, Li W, Tan X. 2012 Microfabrication of IPMC cilia for bio-inspired flow sensing. *Proc. SPIE Electroactive Polymer Actuators and Devices* (*EAPAD 2012*) **8340**, 83401A.